Inorg. Chem. **2007**, *46*, 5023–5033

Osmium NAMI-A Analogues: Synthesis, Structural and Spectroscopic Characterization, and Antiproliferative Properties

Berta Cebrián-Losantos, Artem A. Krokhin, Iryna N. Stepanenko, Rene Eichinger, Michael A. Jakupec, Vladimir B. Arion,* and Bernhard K. Keppler*

Institute of Inorganic Chemistry, Faculty of Chemistry, University of Vienna, Währingerstrasse 42, A-1090 Vienna, Austria

Received March 2, 2007

The osmium(III) complex $[(DMSO)_2H][trans\text{-}Os^{III}Cl_4(DMSO)_2]$ (**1**) has been prepared via stepwise reduction of OsO_4 in concentrated HCl using $N_2H_4 \cdot 2HCl$ and $SnCl_2 \cdot 2H_2O$ in DMSO. **1** reacts with a number of azole ligands, namely, indazole (Hind), pyrazole (Hpz), benzimidazole (Hbzim), imidazole (Him), and 1*H*-1,2,4-triazole (Htrz), in organic solvents, affording novel complexes $(H_2ind)[Os^{III}Cl_4(Hind)(DMSO)]$ (**2**), $(H_2pz)[Os^{III}Cl_4(Hpz)(DMSO)]$ (**3**), $(H_2bzim)[Os^{III}Cl_4(Hbzim)(DMSO)]$ (**4**), $(H_2im)[Os^{III}Cl_4(Him)(DMSO)]$ (**6**), and $(H_2trz)[Os^{III}Cl_4(Htrz)(DMSO)]$ (**7**), which are close analogues of the antimetastatic complex NAMI-A. Metathesis reaction of **4** with benzyltriphenylphosphonium chloride in methanol led to the formation of $(Ph_3PCH_2Ph)[Os^{III}Cl_4(Hbzim)(DMSO)]$ (**5**). The complexes were characterized by IR, UV–vis, ESI mass spectrometry, ^1H NMR spectroscopy, cyclic voltammetry, and X-ray crystallography. In contrast to NAMI-A, **2**–**4**, **6**, and **7** are kinetically stable in aqueous solution and resistant to hydrolysis. Surprisingly, they show reasonable antiproliferative activity in vitro in two human cell lines, HT-29 (colon carcinoma) and SK-BR-3 (mammary carcinoma), when compared with analogous ruthenium compounds. Structure–activity relationships and the potential of the prepared complexes for further development are discussed.

Introduction

Current interest in ruthenium antitumor drugs was stimulated by recent phase I clinical studies of two complexes, namely, $(H_2im)[trans\text{-}RuCl_4(Him)(DMSO)]$ (NAMI-A)[1] and $(H_2ind)[trans\text{-}RuCl_4(Hind)_2]$ (KP1019, FFC14),[2] the first as an agent, which inhibits the process of metastasis formation, and the second as an effective means against primary tumors and metastases, in particular, among others, colon carcinomas. The quest for novel ruthenium compounds with potential antitumor properties has led to synthesis of a large variety of arene complexes with piano-stool structure of the type $[(\eta^6\text{-arene})Ru(L-L)Cl]X$, where arene is biphenyl, benzene, or *p*-cymene, and L−L is ethylenediamine or acetylacetone, and X is a counterion.[3] The complexes showed antitumor activity both in vitro and in vivo, which in some cases was comparable with that of cisplatin and carboplatin. One of the reasons is an optimal chemical reactivity of these compounds under physiological conditions. Certain isostructural osmium analogues, for example $[(\eta^6\text{-biphenyl})Os(en)Cl]BF_4$, which enter substitution reactions much more slowly than the corresponding ruthenium complexes, were found to be inactive in A2780 ovarian cancer cells.[4]

Quite recently Sadler et al.[5] have demonstrated that the reactivity of osmium complexes, particularly the hydrolysis and nucleobase binding, can be effectively tuned by systematic variation of ancillary ligands. The same authors expressed the opinion that in using this approach the design and synthesis of osmium complexes with potential antitumor properties can be realized. Nevertheless, studies on the antitumor activity of osmium complexes are still very scarce.[4,6–8]

* To whom correspondence should be addressed. E-mail: vladimir.arion@univie.ac.at (V.B.A.), bernhard.keppler@univie.ac.at (B.K.K.).

(1) Alessio, E.; Mestroni, G.; Bergamo, B.; Sava, G. *Curr. Top. Med. Chem.* **2004**, *4*, 1525−1535.
(2) Hartinger, C. G.; Zorbas-Seifried, S.; Jakupec, M. A.; Kynast, B.; Zorbas, H.; Keppler, B. K. *J. Inorg. Biochem.* **2006**, *100*, 891−904.
(3) (a) Morris, R. E.; Aird, R. E.; Murdoch, P. D. S.; Chen, H.; Cummings, J.; Hughes, N. D.; Parsons, S.; Parkin, A.; Boyd, G.; Jodrell, D. I.; Sadler, P. J. *J. Med. Chem.* **2001**, *44*, 3616−3621. (b) Aird, R. E.; Cummings, J.; Ritchie, A. A.; Muir, M.; Morris, R. E.; Chen, H.; Sadler, P. J.; Jodrell, D. I. *Br. J. Cancer* **2002**, *86*, 1652−1657.
(4) Dorcier, A.; Dyson, P. J.; Gossens, C.; Rothlisberger, U.; Scopelliti, R.; Tavernelli, I. *Organometallics* **2005**, *24*, 2114−2123.
(5) Peacock, A. F. A.; Habtemariam, A.; Fernandez, R.; Walland, V.; Fabbiani, F. P. A.; Parsons, S.; Aird, R. E.; Jodrell, D. I.; Sadler, P. J. *J. Am. Chem. Soc.* **2006**, *128*, 1739−1748.

10.1021/ic700405y CCC: $37.00
Published on Web 05/12/2007

Attempts to extend the synthetic work onto synthesis of NAMI-A type complexes with metal ions other than ruthenium have also been undertaken and are well documented in the literature. In particular, complexes of rhodium(III) and iridium(III) have been synthesized and their properties have been investigated.[9,10]

Biochemical and cell biological studies show reactivity and cytotoxicity profiles different from those of ruthenium(III) NAMI-A type compounds. In particular, the complexes neither bind strongly to bovine serum albumin nor inhibit markedly the proliferation of human tumor cell lines. Surprisingly, osmium analogues of NAMI-A have not been reported so far, although their synthesis and comparison with ruthenium compounds appears to be more desirable from the point of view of the position of these metals in the periodic table. The evaluation of NAMI-A analogues with metals other than ruthenium, specifically those of osmium(III), has been mainly hindered by synthetic limitations. The synthesis of NAMI-A and related rhodium(III) and iridium(III) compounds was straightforwardly realized because of the availability of starting compounds $[(DMSO)_2H]$ [*trans*-$MCl_4(DMSO)_2$] (M = Ru, Rh, Ir).[11,12] The reaction of these compounds with azole ligands in organic solvents enabled the synthesis of the desired compound families in good yields. Although evidence for the formation of [*trans*-$OsCl_4(DMSO)_2]^-$ (**1**) in solution was reported,[13] the compound has not been isolated as a solid so far. Being intrigued by this fact, we directed our efforts on (i) the isolation of this osmium compound and its full characterization, (ii) the study of the reactivity of $[(DMSO)_2H]$[*trans*-$OsCl_4(DMSO)_2$] toward azole ligands and full characterization of the resulting osmium analogues of NAMI-A type compounds (Figure 1), (iii) cytotoxicity assays of the novel osmium(III) compounds, and (iv) comparison of hydrolytic stability of the prepared osmium complexes with those of the NAMI-A family of compounds.

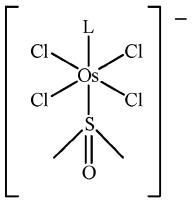

Complex	Counterion	L
1	$H(DMSO)_2^+$	DMSO
2	H_2ind^+	Hind
3	H_2pz^+	Hpz
4	H_2bzim^+	Hbzim
5	$Ph_3PCH_2Ph^+$	Hbzim
6	H_2im^+	Him
7	H_2trz^+	Htrz

Figure 1. Anticancer osmium(III) NAMI-A analogues; underlined complexes have been characterized in this work by X-ray crystallography.

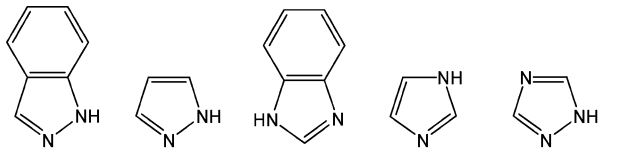

Figure 2. Heterocyclic azole ligands.

We show in this article that $[(DMSO)_2H]$[*trans*-$Os^{III}Cl_4(DMSO)_2$] can be efficiently prepared by stepwise reduction of OsO_4 with hydrazine dihydrochloride in concentrated HCl to Os^{IV} [14] and then with $SnCl_2{\cdot}2H_2O$/DMSO to Os^{III} and Os^{II}.[15] We also describe the nearest congeners, resulting from reactions of $[(DMSO)_2H]$[*trans*-$OsCl_4(DMSO)_2$] with azole ligands (Figure 2), that are closely related to the well-characterized NAMI-A type ruthenium(III) compounds[16−18] with a d^5 low-spin electronic configuration and show that osmium(III) complexes are also worth being investigated as potential antitumor drugs.

Experimental Section

Chemicals. OsO_4 (99.8%) was purchased from Johnson Matthey in 1 g ampoules, $N_2H_4{\cdot}2HCl$ from Fluka, and $SnCl_2{\cdot}2H_2O$ from Merck. The azole ligands, indazole, pyrazole, imidazole, benzimidazole, and 1*H*-1,2,4-triazole, were from Aldrich. 9-Methyladenine (MeAde) was prepared as reported in the literature.[19]

Synthesis of Complexes. *trans*-$Os^{II}Cl_2(DMSO)_4$ and $[(DMSO)_2H]$[*trans*-$Os^{III}Cl_4(DMSO)_2$] (1). $N_2H_4{\cdot}2HCl$ (0.42 g, 4.00 mmol) was added to OsO_4 (1.00 g, 3.93 mmol) in HCl (37%, 25 mL) and

(6) Dorcier, A.; Ang, W. H.; Bolaño, S.; Gonsalvi, L.; Juillerat-Jeannerat, L.; Laurenczy, G.; Peruzzini, M.; Phillips, A. D.; Zanobini, F.; Dyson, P. J. *Organometallics* **2006**, *25*, 4090−4096.
(7) (a) Craciunescu, D. G.; Molina, C.; Parrondo-Iglesias, E.; Alonso, M. P.; Doadrio-Villarejo, J. C.; Gutierrez Rios, M. T.; De Frutos, M. I.; Certad Fombona, G.; Gaston de Iriarte, E. *An. Real Acad. Farm.* **1991**, *57*, 221−240. (b) Doadrio, A.; Craciunescu, D.; Ghirvu, C.; Nuno, J. C. *An. Quim.* **1977**, *73*, 1220−1223. (b) Craciunescu, D. G.; Parrondo Iglesias, E.; Alonso, M. P.; Molina, C.; Doadrio Lopez, A.; Gomez, A.; Mosquerra, R. M.; Ghirvu, C.; Gaston de Iriarte, E. *An. R. Acad. Farm.* **1988**, *54*, 16−45. (c) Craciunescu, D. G.; Molina, C.; Parrondo-Iglesias, E.; Alonso, M. P.; Doadrio-Villarejo, J. C.; Gutierrez Rios, M. T.; De Frutos, M. I.; De Iriarte, E.; Gaston Fombona, G. C.; Ercoli, N. *An. R. Acad. Farm.* **1992**, *58*, 207−231.
(8) Peacock, A. F. A.; Parsons, S.; Sadler, P. J. *J. Am. Chem. Soc.* **2007**, *129*, 3348−3357.
(9) Mestroni, G.; Alessio, E.; Sessanta o Santi, A.; Geremia, S.; Bergamo, A.; Sava, G.; Boccarelli, A.; Schettino, A.; Coluccia, M. *Inorg. Chim. Acta* **1998**, *273*, 62−71.
(10) Messori, L.; Marcon, J.; Orioli, P.; Fontani, M.; Zanello, P.; Bergamo, A.; Sava, G.; Mura, P. *J. Inorg. Biochem.* **2003**, *95*, 37−46.
(11) (a) Alessio, E.; Balducci, G.; Calligaris, M.; Costa, G.; Attia, W. M.; Mestroni, G. *Inorg. Chem.* **1991**, *30*, 609−618. (b) Alessio, E.; Sessanta o Santi, A.; Faleschini, P.; Calligaris, M.; Mestroni, G. *J. Chem. Soc., Dalton Trans.* **1994**, *13*, 1849−1855. (c) Haddad, Y. M. Y.; Henbest, H. B.; Trocha-Grimshaw, J. *J. Chem. Soc., Perkin Trans. 1* **1974**, *5*, 592−595.
(12) Jaswal, J. S.; Rettig, S. J.; James, B. R. *Can. J. Chem.* **1990**, *68*, 1808−1817.
(13) (a) Komozin, P. N. *Zh. Neorg. Khim.* **2000**, *45*, 662−674. (b) Komozin, P. N. *Zh. Neorg. Khim.* **1998**, *43*, 547−553.
(14) Brauer, G. *Handbuch der Präparativen Anorganischen Chemie;* Bd. III, 1981; pp 1742−1744.
(15) McDonagh, A. M.; Humphrey, M. G.; Hockless, D. C. R. *Tetrahedron: Asymmetry* **1997**, *8*, 3579−3583.
(16) (a) Reisner, E.; Arion, V. B.; Guedes da Silva, M. F. C.; Lichtenecker, R.; Eichinger, A.; Keppler, B. K.; Kukushkin, V.; Yu Pombeiro, A. J. L. *Inorg. Chem.* **2004**, *43*, 7083−7093.
(17) (a) Alessio, E.; Balducci, G.; Lutman, A.; Mestroni, G.; Calligaris, M.; Attia, W. M. *Inorg. Chim. Acta* **1993**, *203*, 205−217. (b) Mura, P.; Camalli, M.; Messori, L.; Piccioli, F.; Zanello, P.; Corsini, M. *Inorg. Chem.* **2004**, *43*, 3863−3870.
(18) Alessio, E.; Mestroni, G.; Pacor, S.; Sava, G.; Spinelli, S. *PCT Int. Appl.* WO 9013553, **1990**.
(19) (a) Talman, E. G.; Bruening, W.; Reedijk, J.; Spek, A. L.; Veldman, N. *Inorg. Chem.* **1997**, *36*, 854−861. (b) Charland, J. P.; Phan Viet, M. T.; St-Jacques, M.; Beauchamp, A. L. *J. Am. Chem. Soc.* **1985**, *107*, 8202−8211.

water (3 mL). The solution was stirred at room temperature for 7 days. Afterward, the solvent was removed by rotary evaporation under reduced pressure at 60 °C. To the red residue, $SnCl_2 \cdot 2H_2O$ (0.80 g, 3.54 mmol) and DMSO (8 mL) were added, and the solution was held at 87 °C for 1 h. The precipitated yellow solid *trans*-$Os^{II}Cl_2(DMSO)_4$ was filtered off, washed with acetone (4 × 15 mL) and Et_2O (4 × 15 mL), and dried in vacuo. The IR spectrum of this compound was identical to that of *trans*-$OsCl_2(DMSO)_4$ prepared as described in the literature.[15] The filtrate was allowed to stand at room temperature overnight, producing yellow-orange crystals of the product. These were separated by filtration and dried in vacuo. Yield: *trans*-$Os^{II}Cl_2(DMSO)_4$ 0.34−0.56 g, 15−25%; $[(DMSO)_2H][trans\text{-}Os^{III}Cl_4(DMSO)_2]$ 0.50−0.76 g, 20−30%. Anal. Calcd for $C_8H_{25}Cl_4O_4OsS_4$ (M_r = 645.59 g/mol): C, 14.88; H, 3.90; S, 19.87; Cl, 21.97. Found: C, 14.63; H, 3.79; S, 19.67; Cl, 21.67. ESI−MS in MeOH (negative): *m/z* 488 $[Os^{III}Cl_4(DMSO)_2]^-$, 410 $[Os^{III}Cl_4(DMSO)]^-$, 332 $[Os^{III}Cl_4]^-$. IR (KBr), selected bands, cm^{-1}: 416 (w), ν(Os−S); 909 (vw), 916 (vw), 936 (w), 947 (w), 969 (vw), 977 (vw), 1017 (s), $\rho(CH_3)$; 1080 (s), ν(S═O); 1292 (vw), 1304 (vw), 1318 (w), $\delta(CH_3)$. UV−vis (MeOH), λ_{max}, nm (ϵ, M^{-1} cm^{-1}): 419 (351) sh, 348 (4189), 268 (5077) sh. UV−vis (H_2O), λ_{max}, nm (ϵ, M^{-1} cm^{-1}): 410 (666) sh, 374 (2516) sh, 344 (6162), 300 (757) sh, 257 (1174). Suitable crystals for X-ray diffraction study were selected directly from the reaction vessel.

(H_2ind)[*trans*-$Os^{III}Cl_4$(Hind)(DMSO)] (2). Indazole (0.04 g, 0.31 mmol) was added to **1** (0.10 g, 0.15 mmol) in dry ethanol (10 mL), and the mixture was held at 53 °C for 2 h. The orange-red solution was filtered to remove solid impurities and then evaporated almost completely under reduced pressure. Addition of hexane to the remaining residue led to the formation of red crystals, which were filtered off, washed with diethyl ether (5 mL), and dried in vacuo. Yield: 0.05 g, 50%. Anal. Calcd for $C_{16}H_{19}Cl_4N_4OOsS$ (M_r = 647.45 g/mol): C, 29.68; H, 2.96; N, 8.65; S, 4.95. Found: C, 29.26; H, 2.96; N, 8.35; S, 4.83. ESI−MS in MeOH (negative): *m/z* 528 $[Os^{III}Cl_4(Hind)(DMSO)]^-$, 410 $[Os^{III}Cl_4(DMSO)]^-$, 332 $[Os^{III}Cl_4]^-$. IR (KBr), selected bands, cm^{-1}: 432 (w), ν(Os−S); 1023 (m), $\rho(CH_3)$; 1058 (vs), ν(S═O). UV−vis (MeOH), λ_{max}, nm (ϵ, M^{-1} cm^{-1}): 378 (1650), 332 (7317), 298 (21 255) sh. UV−vis (H_2O), λ_{max}, nm (ϵ, M^{-1} cm^{-1}): 408 (168) sh, 370 (330), 330 (815), 296 (1361) sh, 285 (1485), 258 (1260). X-ray diffraction-quality crystals were grown by vapor diffusion of *n*-hexane into a saturated EtOH solution of the complex.

(H_2pz)[*trans*-$Os^{III}Cl_4$(Hpz)(DMSO)] (3). Pyrazole (0.025 g, 0.37 mmol) was added to **1** (0.10 g, 0.15 mmol) in dry methanol (10 mL), and the mixture was held at 53 °C for 2 h. Afterward the yellow solution was evaporated under reduced pressure, and diethyl ether was added dropwise. The resulting red crystals were filtered off, washed with diethyl ether (5 mL), and dried in vacuo. Yield: 0.05 g, 60%. Anal. Calcd for $C_8H_{15}Cl_4N_4OOsS$ (M_r = 547.34 g/mol): C, 17.55; H, 2.76; N, 10.24; S, 5.86. Found: C, 17.62; H, 2.69; N, 10.23; S, 5.95. ESI−MS in MeOH (negative): *m/z* 478 $[Os^{III}Cl_4(Hpz)(DMSO)]^-$, 410 $[Os^{III}Cl_4(DMSO)]^-$, 332 $[Os^{III}Cl_4]^-$. IR (KBr), selected bands, cm^{-1}: 436 (w), ν(Os−S); 1016 (s), $\rho(CH_3)$; 1056 (s), ν(S═O). UV−vis (MeOH), λ_{max}, nm (ϵ, M^{-1} cm^{-1}): 377 (330), 335 (5280). UV−vis (H_2O), λ_{max}, nm (ϵ, M^{-1} cm^{-1}): 408 (237) sh, 372 (1168), 330 (4865), 236 (6568). Suitable crystals for X-ray diffraction study were selected directly from the reaction vessel.

(H_2bzim)[*trans*-$Os^{III}Cl_4$(Hbzim)(DMSO)] (4). Benzimidazole (0.05 g, 0.45 mmol) was added to a suspension of **1** (0.10 g, 0.15 mmol) in acetone (10 mL), and the mixture was held at 53 °C for 2 h. The clear solution formed on heating produced a yellow solid, which was filtered off, washed with acetone (2 × 5 mL), diethyl ether (5 mL), and dried in vacuo. Yield: 0.06 g, 60%. Anal. Calcd for $C_{16}H_{19}Cl_4N_4OOsS$ (M_r = 647.45 g/mol): C, 29.68; H, 2.96; N, 8.65; S, 4.95. Found: C, 29.61; H, 3.04; N, 8.47; S, 4.82. ESI−MS in MeOH (negative): *m/z* 528 $[Os^{III}Cl_4(Hbzim)(DMSO)]^-$, 410 $[Os^{III}Cl_4(DMSO)]^-$, 332 $[Os^{III}Cl_4]^-$. IR (KBr), selected bands, cm^{-1}: 426 (w), ν(Os−S); 1016 (s), $\rho(CH_3)$; 1067 (vs), ν(S═O). UV−vis (MeOH), λ_{max}, nm (ϵ, M^{-1} cm^{-1}): 377 (1186), 334 (6324), 279 (13 747) sh, 273 (19 763), 267 (20 553). UV−vis (H_2O), λ_{max}, nm (ϵ, M^{-1} cm^{-1}): 406 (599) sh, 370 (1367), 330 (5096), 277 (11690), 270 (13 488), 250 (11 091) sh.

(Ph_3PCH_2Ph)[*trans*-$Os^{III}Cl_4$(Hbzim)(DMSO)] (5). Benzyltriphenylphosphonium chloride (0.06 g, 0.15 mmol) was added to a solution of **4** (0.05 g, 0.10 mmol) in methanol (20 mL), and the mixture was stirred at room temperature for 2 h. Slow removal of solvent by rotary evaporation under reduced pressure led to precipitation of a yellow solid, which was filtered off, washed with diethyl ether (2 × 5 mL), and dried in vacuo. Yield: 0.05 g, 60%. Anal. Calcd for $C_{34}H_{34}Cl_4N_2OOsPS$ (M_r = 881.73 g/mol): C, 46.31; H, 3.89; N, 3.18. Found: C, 46.61; H, 3.64; N, 3.17. ESI−MS in MeOH (negative): *m/z* 528 $[Os^{III}Cl_4(Hbzim)(DMSO)]^-$, 410 $[Os^{III}Cl_4(DMSO)]^-$, 332 $[Os^{III}Cl_4]^-$. ESI−MS in MeOH (positive): *m/z* 353, $[Ph_3PCH_2Ph]^+$. X-ray diffraction-quality crystals were grown by slow diffusion of methanol solutions of **4** and benzyltriphenylphosphonium chloride in an H-tube.

(H_2im)[*trans*-$Os^{III}Cl_4$(Him)(DMSO)] (6). Imidazole (0.03 g, 0.45 mmol) was added to a suspension of **1** (0.10 g, 0.15 mmol) in acetone (10 mL), and the mixture was held at 53 °C for 20 h. The reaction mixture was cooled to room temperature, and the yellow solid was filtered off, washed with acetone (2 × 5 mL) and diethyl ether (5 mL), and dried in vacuo. Yield: 0.07 g, 80%. Anal. Calcd for $C_8H_{15}Cl_4N_4OOsS$ (M_r = 547.34 g/mol): C, 17.55; H, 2.76; N, 10.24; S, 5.85; Found: C, 17.61; H, 2.64; N, 10.18; S, 5.47. ESI−MS in MeOH (negative): *m/z* 478 $[Os^{III}Cl_4(Him)(DMSO)]^-$, 410 $[Os^{III}Cl_4(DMSO)]^-$, 332 $[Os^{III}Cl_4]^-$. IR (KBr), selected bands, cm^{-1}: 435 (m), ν(Os−S); 1016 (s), $\rho(CH_3)$; 1065 (vs), ν(S═O). UV−vis (MeOH), λ_{max}, nm (ϵ, M^{-1} cm^{-1}): 373 (869), 334 (3913). UV−vis (H_2O), λ_{max}, nm (ϵ, M^{-1} cm^{-1}): 409 (192) sh, 371 (1275), 330 (4996), 254 (2025). X-ray diffraction-quality crystals of **6**·0.5EtOH were grown by vapor diffusion of diethyl ether into an ethanol solution of the complex.

(H_2trz)[*trans*-$Os^{III}Cl_4$(Htrz)(DMSO)] (7). 1-*H*-1,2,4-Triazole (0.03 g, 0.45 mmol) was added to a suspension of **1** (0.10 g, 0.15 mmol) in acetone (10 mL), and the mixture was held at 53 °C for 1 h. A clear solution formed on heating produced a yellow solid, which was filtered off, washed with acetone (2 × 5 mL) and diethyl ether (5 mL), and dried in vacuo. Yield: 0.05 g, 60%. Anal. Calcd for $C_6H_{13}Cl_4N_6OOsS$ (M_r = 549.31 g/mol): C, 13.12; H, 2.38; N, 15.30; S, 5.84. Found: C, 13.32; H, 2.31; N, 15.61; S, 5.81. ESI−MS in MeOH (negative): *m/z* 479 $[Os^{III}Cl_4(Htrz)(DMSO)]^-$, 410 $[Os^{III}Cl_4(DMSO)]^-$, 332 $[Os^{III}Cl_4]^-$. IR (KBr), selected bands, cm^{-1}: 434 (m), ν(Os−S); 1026 (br), $\rho(CH_3)$; 1057 (vs), ν(S═O). UV−vis (MeOH), λ_{max}, nm (ϵ, M^{-1} cm^{-1}): 370 (2778), 336 (5555). UV−vis (H_2O), λ_{max}, nm (ϵ, M^{-1} cm^{-1}): 409 (329) sh, 371 (2983), 333 (5786), 256 (2026). X-ray diffraction-quality crystals were grown by vapor diffusion of diethyl ether into a methanol solution of the complex.

Physical Measurements. Elemental analyses were carried out at the Microanalytical Service of the Institute of Physical Chemistry of the University of Vienna. Infrared spectra were obtained from KBr pellets with a Perkin-Elmer 370 FTIR 2000 instrument (4000−400 cm^{-1}). UV−vis spectra were recorded on a Perkin-Elmer Lambda 20 UV−vis spectrophotometer using samples dissolved

Table 1. Crystal Data and Details of Data Collection for **1**−**3** and **5**−**7**

complex	**1**	**2**	**3**	**5**	**6**·0.5EtOH	**7**
empirical formula	$C_8H_{25}Cl_4O_4OsS_4$	$C_{16}H_{19}Cl_4N_4OOsS$	$C_8H_{15}Cl_4N_4OOsS$	$C_{34}H_{34}Cl_4N_2OOsPS$	$C_9H_{18}Cl_4N_4O_{1.5}OsS$	$C_6H_{13}Cl_4N_6OOsS$
fw	645.59	647.45	547.34	881.73	570.37	549.31
space group	$P\bar{1}$	$P2_1/n$	$P2_1/c$	$P2_1/n$	$P2_1/c$	$P\bar{1}$
a (Å)	9.1652(4)	10.5903(4)	8.4670(2)	10.6249(17)	10.1758(4)	7.4444(4)
b (Å)	13.8866(14)	8.6393(3)	14.9489(4)	15.416(3)	16.1069(7)	8.0206(4)
c (Å)	16.4116(8)	22.6247(9)	13.0000(3)	20.809(3)	20.9749(9)	13.1209(7)
α (deg)	90.201(5)					92.973(3)
β (deg)	90.130(2)	103.068(2)	97.585(1)	93.677(10)	92.605(3)	103.329(3)
γ (deg)	100.651(1)					93.293(3)
V (Å^3)	2052.8(2)	2016.39(13)	1631.04(7)	3401.5(9)	3434.2(2)	759.36(7)
Z	4	4	4	4	8	2
λ (Å)	0.71073	0.71073	0.71073	0.71073	0.71073	0.71073
ρ_{calcd} (g cm^{-3})	2.089	2.133	2.229	1.722	2.206	2.402
cryst size (mm^3)	0.20 × 0.10 × 0.08	0.26 × 0.20 × 0.06	0.14 × 0.14 × 0.14	0.36 × 0.26 × 0.14	0.16 × 0.05 × 0.02	0.18 × 0.14 × 0.12
T (K)	100	100	296	296	100	100
μ (cm^{-1})	71.47	69.73	85.97	42.03	81.73	92.37
R1[a]	0.0320	0.0212	0.0183	0.0271	0.0328	0.0201
wR2[b]	0.0845	0.0577	0.0358	0.0617	0.0627	0.0451
GOF[c]	1.094	1.048	1.026	1.005	1.029	1.010

[a] $R1 = \sum||F_o| - |F_c||/\sum|F_o|$. [b] $wR2 = \{\sum[w(F_o^2 - F_c^2)^2]/\sum[w(F_o^2)^2]\}^{1/2}$. [c] $GOF = \{\sum[w(F_o^2 - F_c^2)^2]/(n - p)\}^{1/2}$, where n is the number of reflections, and p is the total number of parameters refined.

in methanol or in water at 298 K. The aqueous solution behavior with respect to hydrolysis of **2**−**4**, **6**, and **7** was studied at 298 K over 48 h by UV−vis spectroscopy. Electrospray ionization mass spectrometry was carried out with a Bruker Esquire 3000 instrument (Bruker Daltonic, Bremen, Germany) in methanol and methanol/water (30/70). Expected and experimental isotope distributions were compared. The ^{1}H NMR spectra were recorded at 400.13 MHz on a Bruker DPX400 (Ultrashield Magnet) spectrometer. The solution behavior of **6** was studied by ^{1}H NMR in aqueous solution (D_2O, pH ∼5.5, 37 °C) for 2 days and in physiological medium (phosphate buffer 0.05 M, pH 7.4; 0.15 M NaCl, 37 °C) for 3 days. The interaction of **6** with 9-methyladenine (1:1.5 molar ratio) in phosphate buffer (pH 6.0, 37 °C) was followed by ^{1}H NMR spectroscopy for 4 days. Acetone (1 μL/mL) was used as reference for the NMR experiments. Cyclic voltammograms were measured in a two-compartment three-electrode cell using a 1.0-mm-diameter glassy-carbon-disk working electrode, probed by a Luggin capillary, and connected to a silver-wire pseudoreference electrode and a platinum auxiliary electrode. Measurements were performed at room temperature using an EG & G PARC 273A potentiostat/galvanostat. Deaeration of solutions was accomplished by passing a stream of argon through the solution for 10 min prior to the measurements and then maintaining a blanket atmosphere of argon over the solution during the measurements. The potentials were measured in 0.2 M phosphate buffer solutions (pH 7.0), using methyl viologen ($E^{ox}_{1/2} = -0.44$ V vs NHE in water)[20] as an internal standard and are quoted relative to NHE.

Crystallographic Structure Determination. X-ray diffraction measurements were performed on an X8APEX II CCD diffractometer at 100 or 296 K. Single crystals were positioned at 37.5, 40, 37.5, 40, 40, and 40 mm from the detector, and 1793, 5247, 1134, 948, 3201, and 1973 frames were measured, each for 20, 5, 60, 8, 50, and 3 s over a 1° scan width for **1**−**3** and **5**−**7**, correspondingly. The data were processed using SAINT software.[21] Crystal data, data collection parameters, and structure refinement details for **1**−**3** and **5**−**7** are given in Table 1. The structures were solved by direct methods and refined by full-matrix least-squares techniques. Non-hydrogen atoms were refined with anisotropic displacement parameters. H atoms were placed at calculated positions and refined as riding atoms in the subsequent least-squares model refinements. The isotropic thermal parameters were estimated to be 1.2 times the values of the equivalent isotropic thermal parameters of the non-hydrogen atoms to which hydrogen atoms are bonded. The following computer programs were used: structure solution, SHELXS-97;[22] refinement, SHELXL-97;[23] molecular diagrams, ORTEP;[24] computer, Pentium IV. Scattering factors were taken from the literature.[25]

Cell Lines and Culture Conditions. Human HT-29 (colon carcinoma) and SK-BR-3 (mammary carcinoma) cells were kindly provided by Brigitte Marian (Institute of Cancer Research, Medical University of Vienna, Austria) and Evelyn Dittrich (General Hospital, Medical University of Vienna, Austria), respectively. All of the cell culture media and supplements were purchased from Sigma-Aldrich, Vienna, Austria, unless indicated otherwise. Cells were grown in 75 cm^2 culture flasks (Iwaki/Asahi Technoglass, Gyouda, Japan) as adherent monolayer cultures in complete culture medium, that is, minimal essential medium (MEM) supplemented with 10% heat-inactivated fetal bovine serum (Invitrogen, Paisley, U.K.), 1 mM sodium pyruvate, 4 mM l-glutamine, and 1% non-essential amino acids (100×). Cultures were maintained at 37 °C in a humidified atmosphere containing 5% CO_2.

Cytotoxicity Tests in Cancer Cell Lines. Cytotoxicity was determined by means of the colorimetric MTT assay (MTT = 3-(4,5-dimethyl-2-thiazolyl)-2,5-diphenyl-2H-tetrazolium bromide; purchased from Fluka, Vienna, Austria). HT-29 and SK-BR-3 cells were harvested from culture flasks by trypsinization and seeded into 96-well microculture plates (Iwaki/Asahi Technoglass, Gyouda, Japan). A seeding density of 4 × 10^3 cells/well was chosen to ensure exponential growth throughout drug exposure. After a 24 h

(20) Guedes da Silva, M. F. C.; Pombeiro, A. J. L.; Geremia, S.; Zangrando, E.; Calligaris, M.; Zinchenko, A. V.; Kukushkin, V. Yu. *J. Chem. Soc., Dalton Trans.* **2000**, 1363−1371.
(21) *SAINT-Plus*, version 7.06a and APEX2; Bruker-Nonius AXS Inc.: Madison, WI, 2004.
(22) Sheldrick, G. M. *SHELXS-97, Program for Crystal Structure Solution*; University of Göttingen, Germany, 1997.
(23) Sheldrick, G. M. *SHELXL-97, Program for Crystal Structure Refinement*; University of Göttingen: Göttingen, Germany, 1997.
(24) Johnson, C. K. *Report ORNL-5138;* Oak Ridge National Laboratory: Oak Ridge, TN, 1976.
(25) *International Tables for X-ray Crystallography*; Kluwer Academic Press: Dordrecht, The Netherlands, 1992; Vol. C, Tables 4.2.6.8 and 6.1.1.4.

preincubation, cells were exposed to solutions of the test compounds in 200 μL/well complete culture medium for 96 h. At the end of exposure, drug solutions were replaced by 100 μL/well RPMI1640 culture medium (supplemented with 10% heat-inactivated fetal bovine serum) plus 20 μL/well MTT solution (5 mg/mL) in phosphate-buffered saline. After incubation for 4 h, the medium/MTT mixtures were removed, and the formazan crystals formed by the mitochondrial dehydrogenase activity of vital cells were dissolved in 150 μL DMSO per well. Optical densities at 550 nm were measured with a microplate reader (Tecan Spectra Classic), using a reference wavelength of 690 nm to correct for unspecific absorption. The quantity of vital cells was expressed in terms of T/C values by comparison to untreated control microcultures, and IC_{50} values were calculated from concentration−effect curves by interpolation. Evaluation is based on the means from at least three independent experiments, each comprising six microcultures per concentration level.

Results and Discussion

Synthesis and Characterization of the Complexes. 1 was synthesized by two consecutive reductions. The first one is the reduction of $Os^{VIII}O_4$ to $[Os^{IV}Cl_6]^{2-}$ by hydrazine dihydrochloride in the presence of concentrated HCl, and the second is the reduction of $[Os^{IV}Cl_6]^{2-}$ to Os^{III} and Os^{II} by $SnCl_2{\cdot}2H_2O$ in the presence of dimethyl sulfoxide with the formation of $[(DMSO)_2H][Os^{III}Cl_4(DMSO)_2]$ (20−30%) and *trans*-$Os^{II}Cl_2(DMSO)_4$ (15−25%). *trans*-$Os^{II}Cl_2(DMSO)_4$,[15] which precipitated first, was filtered off, whereas the filtrate produced nice orange needles of **1**, which were suitable for X-ray crystallography (vide infra). It should be also noted that the related ruthenium(III) complex $[(DMSO)_2H][Ru^{III}Cl_4(DMSO)_2]$ was originally isolated from the mother liquor of *cis*-$Ru^{II}Cl_2(DMSO)_4$.[26] **2**−**4**, **6,** and **7** were synthesized by reaction of $[(DMSO)_2H][trans\text{-}Os^{III}Cl_4(DMSO)_2]$ (**1**) with an excess of the corresponding azole ligand in acetone, ethanol, or methanol by using the destabilizing trans effect of the two axially S-bound π-accepting DMSO ligands in **1**, whereas **5** was obtained by metathesis reaction of $(H_2bzim)[trans\text{-}Os^{III}Cl_4(Hbzim)(DMSO)]$ (**4**) and Ph_3PCH_2PhCl in methanol. The reaction of $[(DMSO)_2H][Os^{IV}Cl_5(DMSO)]$[27] with pyrazole in 1:2 molar ratio in isoamylalcohol at 105 °C for 1 h yielded a mixture of different products, one of which was shown by X-ray diffraction to be $(H_2pz)[trans\text{-}Os^{III}Cl_4(Hpz)(DMSO)]$ (**3**).

The infrared spectrum of **1** showed one S═O (S-bonded DMSO) stretching vibration at 1080 cm^{-1} typical for a trans configuration. The lighter congener $[(DMSO)_2H][trans\text{-}Ru^{III}Cl_4(DMSO)_2]$ revealed this vibration at 1082 cm^{-1}.[12] Band assignment was also confirmed by replacement of DMSO with DMSO-d_6. The hydrogen-bridged cation $[(DMSO)_2H]^+$ has been previously discovered for $[(DMSO)_2H][trans\text{-}MCl_4(DMSO)_2]$, where M = Ru,[12] Rh.[28] The IR spectra of these complexes display a very broad band of medium intensity between 1600 and 1100 cm^{-1} and an intense broad band between 900 and 600 cm^{-1}. In **1**, this intense band was found at 844 cm^{-1}, very similar to that for $[(DMSO)_2H]_2[OsCl_6]$[27] (845 cm^{-1}) and was blue shifted when compared to that observed for $[(DMSO)_2H][trans\text{-}Ru^{III}Cl_4(DMSO)_2]$ at 730 cm^{-1}. DMSO possesses rather strong π-acceptor properties and, compared to azole ligands, shows the greater trans-labilizing effect along the vector S−Os−N. As a result, the positions of stretching vibrations Os−S (426−436 cm^{-1}), S═O (S-bonded DMSO) (1056−1067 cm^{-1}), and deformation vibrations C−H (1016−1026 cm^{-1}) in IR spectra of **2**−**4**, **6**, and **7** do not change significantly after the replacement of one azole by another. In the case of starting compound **1**, a mutual labilization of DMSO ligands on the vector S−Os−S expressed in Os−S bond lengthening (2.33 Å (**1**), 2.26−2.27 Å (**2**−**7**)) (Figures 3−8) resulted in the decrease of its strength as evidenced by lowering the absorption frequency ν(Os−S) to 416 cm^{-1} (**1**). The marginal

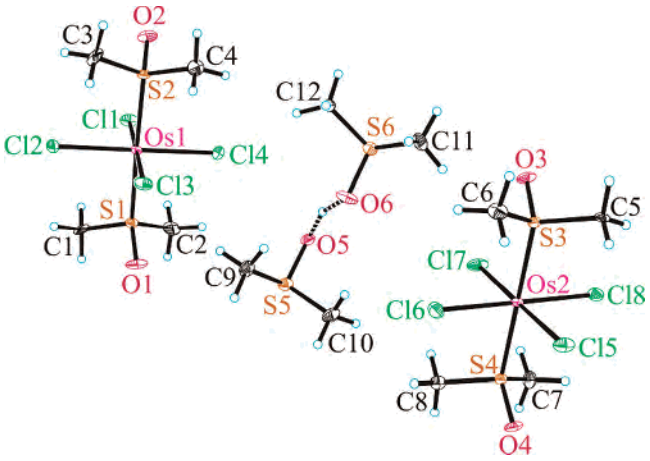

Figure 3. ORTEP diagram of the structure of **1** with atom labeling scheme showing two crystallographically independent complex anions and one $[(DMSO)_2H]^+$ cation. The second cation present in the asymmetric unit was omitted for clarity; thermal ellipsoids were drawn at 50% probability level. Selected bond lengths (Å) and angles (deg): Os1−S1 2.3301(9), Os1−S2 2.3345(9), Os1−Cl1 2.3693(11), Os1−Cl2 2.3629(7), Os1−Cl3 2.3632(10), Os1−Cl4 2.3569(7), Os2−S3 2.3303(10), Os2−S4 2.3364(10), Os2−Cl5 2.3726(9), Os2−Cl6 2.3496(8), Os2−Cl7 2.3490(9), Os2−Cl8 2.3704(8), S1−O1 1.466(3), S2−O2 1.469(3), S3−O3 1.479(3), S4−O4 1.469(3), S5−O5 1.538(3), S6−O6 1.567(3).

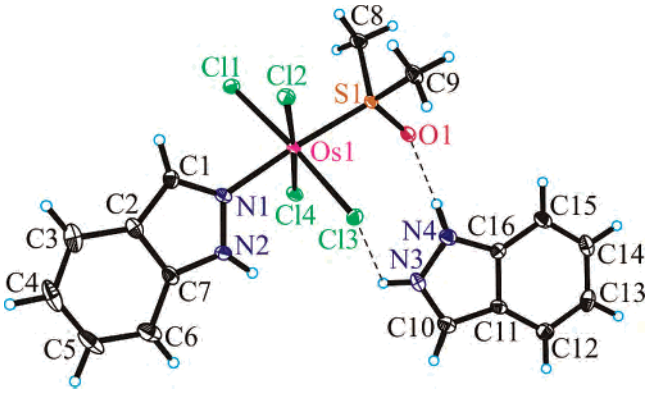

Figure 4. ORTEP view of **2** with atom labeling scheme; the thermal ellipsoids are shown at 50% probability level. Selected bond lengths (Å) and bond angles (deg): Os1−N1 2.090(2), Os1−Cl1 2.3530(7), Os1−Cl2 2.3511(7), Os1−Cl3 2.3603(7), Os1−Cl4 2.3928(7), Os1−S1 2.2690(7), S1−O1 1.495(2) Å, N1−Os1−S1 176.02(6), Cl3−Os1−N1−N2 −39.1(2)°.

(26) Alessio, E.; Mestroni, G.; Nardin, G.; Attia, W. M.; Calligaris, M.; Sava, G.; Zorzet, S. *Inorg. Chem.* **1988**, *27*, 4099−4106.
(27) Rudnitskaya, O. V.; Buslaeva, T. M.; Lyalina, N. N. *Zh. Neorg. Khim.* **1994**, *39*, 922−924.
(28) (a) James, B. R.; Morris, R. H.; Einsten, F. W. B.; Willis, A. *J. Chem. Soc., Chem. Commun.* **1980**, *1*, 31−32. (b) James, B. R.; Morris, R. H. *Can. J. Chem.* **1980**, *58*, 399−408.

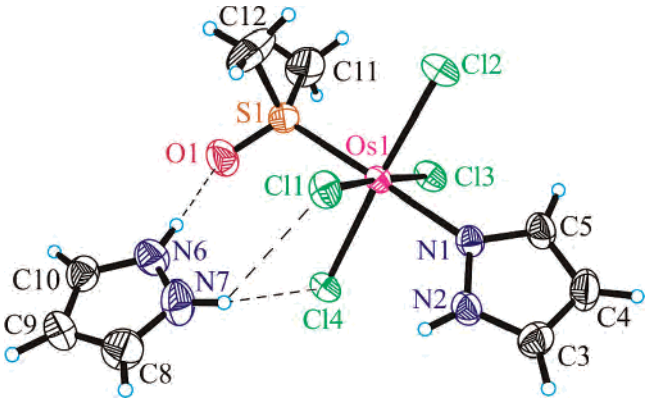

Figure 5. ORTEP view of **3** with atom labeling scheme; the thermal ellipsoids are shown at 50% probability level. Selected bond lengths (Å) and bond angles (deg): Os1−N1 2.109(2), Os1−Cl1 2.3542(6), Os1−Cl2 2.3646(6), Os1−Cl3 2.3591(6), Os1−Cl4 2.3640(6), Os1−S1 2.2656(7), S1−O1 1.482(2) Å, N1−Os1−S1 179.09(5), Cl4−Os1−N1−N2 −40.65(18).

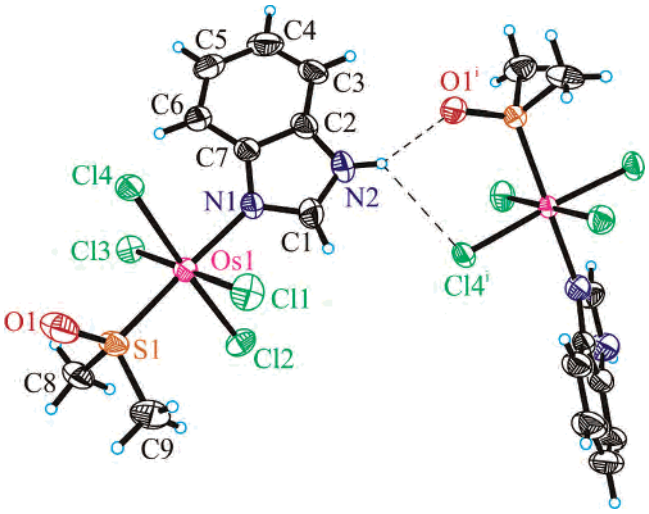

Figure 6. Fragment of the crystal structure of **5** showing the formation of interanionic bifurcated hydrogen bond. Atoms marked with i are at the symmetry positions ($-x + 1.5$, $y + 0.5$, $-z + 1.5$). Selected bond lengths (Å) and angles (deg): Os1−N1 2.120(3), Os1−Cl1 2.3536(9), Os1−Cl2 2.3704(8), Os1−Cl3 2.3604(9), Os1−Cl4 2.3634(8), Os1−S1 2.2632(9), S1−O1 1.475(3) Å, N1−Os1−S1 177.74(8), Cl3−Os1−N1−C7 41.2(3)°.

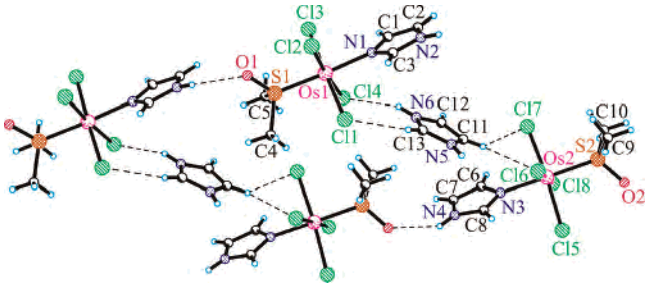

Figure 7. Part of the crystal structure of **6** showing the bridging role of one of the imidazolium cations between two [*trans*-$RuCl_4$(Him)(DMSO)]$^-$ anions. Atoms marked with i are at the symmetry positions ($-x + 1.5$, $y + 0.5$, $-z + 1.5$). Selected bond lengths (Å) and angles (deg): Os1−N1 2.097(4), Os1−Cl1 2.3626(11), Os1−Cl2 2.3494(11), Os1−Cl3 2.3640(11), Os1−Cl4 2.3748(11), Os1−S1 2.2648(11), S1−O1 1.482(3) Å, N1−Os1−S1 177.55(11), N3−Os2−S2 178.96(11), Cl1−Os1−N1−C3 −38.8(4), Cl8−Os2−N3−C6 −37.4(4)°.

shortening of S═O bond length (1.47−1.48 Å (**1**), 1.48−1.49 Å (**2**−**7**)) (Figures 3−8) did not affect the position of the stretching vibration ν(S═O). The general character of

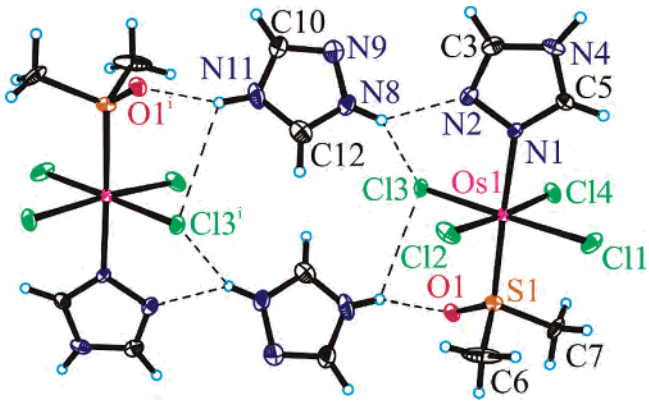

Figure 8. ORTEP view of a centrosymmetric fragment of the crystal structure of **7** with atom labeling scheme; the thermal ellipsoids are shown at 50% probability level. Selected bond lengths (Å) and bond angles (deg): Os1−N1 2.095(3), Os1−Cl1 2.3548(8), Os1−Cl2 2.3724(8), Os1−Cl3 2.3574(8), Os1−Cl4 2.3497(8), Os1−S1 2.2592(8), S1−O1 1.492(2), N1−N2 1.383(4), N2−C3 1.302(4), C3−N4 1.350(4), N4−C5 1.353(4), C5−N1 1.307(4) Å, N1−Os1−S1 177.71(7), Cl3−Os1−N1−N2 39.13(22)°.

IR spectra of **2**−**7** compares well with those of ruthenium NAMI-A analogues.

The electronic absorption spectra of **1** in water and methanol are very similar. The band with an absorption maximum at 348 nm in methanol is slightly blue shifted (344 nm) when water is used as solvent. These results agree well with the spectra for the lighter congener [$(DMSO)_2$H][*trans*-$Ru^{III}Cl_4(DMSO)_2$],[11a] which shows a maximum absorption at 402 (methanol) and 396 nm (water). The bands at 194 and 204 nm for **1** in water are due to the $\pi-\pi^*$ transitions of the DMSO ligands. UV−vis spectra of the aqueous solutions of **2**−**4**, **6**, and **7** are characterized by four absorption bands with maxima near 200 nm ($\pi-\pi^*$ transitions of the ligands) within 236−298, 323−336, 370−378 nm and a shoulder at 406−409 nm. In addition, the second band of **2** and **4** is typical for a free or annelated benzene ring and has an oscillatory character[29] (Table S1). Very weak d−d transitions of octahedral osmium(III) complexes, which are solvent independent, can be observed very rarely because they are obscured by more intense charge transfer absorptions.[30] The observed solvatochromism (a hypsochromic shift (blue) with increasing solvent polarity, in our case the change from methanol to water and a change of band intensity) indicates the presence of metal−ligand charge-transfer (MLCT) bands, which also overlap with intraligand transitions in coordinated azole and DMSO ligands. Taking into consideration the presence of a hole in the t_{2g} subshell of low-spin Os^{III} and the presence of ligands with electron-donating properties in its coordination sphere, the appearance of low-energy LMCT bands is expected. However, there is no clear dependence of charge-transfer energy from the net electron-donor character of the azole ligands (the third and fourth bands for **2**−**4, 6**, and **7** show very close maxima). Just as for [$(DMSO)_2$H][*trans*-$M^{III}Cl_4(DMSO)_2$], upon re-

(29) Lambert, J. B.; Shurvell, H. F.; Lightner, D. A.; Cooks, R. G. *Organic Structural Spectroscopy*; Prentice Hall: Upper Saddle River, NJ, 1998; pp 568.
(30) Lever, A. B. P. *Inorganic Electronic Spectroscopy*, 2nd Ed.; Elsevier: Amsterdam, The Netherlands, 1984; p 862.

placement of Ru^{III} by Os^{III} in all of the NAMI-A analogues, a blue shift of all of the absorption bands with preserved general character of the spectra is observed. This is probably due to the stronger ligand field splitting for third row transition-metal complexes (Table S1).

Crystal Structures. The structures of the complexes reported herein are of interest because of the paucity of documented X-ray diffraction data for osmium(III)-sulfoxide complexes[31] and lack of such data for osmium(III)-azole derivatives.[32] **1** crystallizes in the triclinic space group $P\bar{1}$ with cell parameters very close to those of related Ru, Ir, or Rh compounds, the structures of which were solved in the monoclinic space group $P2/n$. The crystal structure of **1** consists of $[(DMSO)_2H]^+$ cations and [*trans*-$OsCl_4(DMSO)_2]^-$ anions. Figure 3 displays a perspective view of two crystallographically independent complex anions and one of the two independent $[Me_2SO\cdots H\cdots OSMe_2]^+$ cations. Selected bond lengths (Å) and angles (deg) are quoted in the legend to Figure 3. The structure of the $[(DMSO)_2H]^+$ cation is the same as in the complexes $[(DMSO)_2H]$[*trans*-$MCl_4(DMSO)_2$], where M = Ru, Ir, Rh or in $[(DMSO)_2H]$[*trans*-$OsCl_4$-(DMSO)NO].[33]

The osmium(III) ions in [*trans*-$OsCl_4$(Hind)(DMSO)]$^-$ of **2** and in [*trans*-$OsCl_4$(Hpz)(DMSO)]$^-$ of **3** have the expected distorted octahedral coordination geometry (Figures 4 and 5), with four chloride ligands in the equatorial positions and a DMSO molecule bound through its sulfur atom trans to the indazole or pyrazole ligand in axial positions. The Os1−Cl4 and Os1−Cl3 bonds in **2** are significantly longer than Os1−Cl1 and Os1−Cl2 (legend to Figure 4). The elongation of the first two bonds is probably due to the involvement of both Cl4 and Cl3 as proton acceptors in two intermolecular and one intramolecular hydrogen-bonding interactions, respectively, namely, Cl4···H2−N2($-x + 1, -y + 1, -z + 1$) [Cl4···N2 3.336 Å], Cl4···H3−N3($-x + 1, -y + 1, -z + 1$) [Cl4···N3 3.226 Å] and Cl3···H3−N3 (the parameters of this H bond are quoted below). The average value of the Os−Cl bond length in **3** [2.361(2) Å] is close to those found in $[(DMSO)_2H]$[*trans*-$OsCl_4(DMSO)_2$] (**1**) [2.3617(32) Å] and in *mer*-$[OsCl_3(NH_3)_2(Me_2S)]$ [2.368(8) Å].[20] The Os−N1 bond of 2.090(2) and 2.109(2) Å in **2** and **3**, correspondingly, compares well with Ru−N1 in the related complex (H_2ind)[*trans*-$RuCl_4$(Hind)(DMSO)] at 2.0901(13) Å[16a] and is significantly shorter than similar bonds trans to sulfur-bound DMSO in the osmium(II) complexes *trans,cis,cis*-Os^{II}-$Cl_2(Hind)_2(DMSO)_2$ and *trans,cis,cis*-$Os^{II}Cl_2(Hpz)_2(DMSO)_2$ at 2.130(4), 2.137(4) and 2.1202(17), 2.1365(17) Å, respectively.[34] The Os−S1 bond lengths of 2.2690(7) Å (**2**) and 2.2656(7) Å (**3**) (sulfur being trans to the indazole or pyrazole nitrogen) are markedly shorter than those found in $[(DMSO)_2H]$-$[OsCl_4(DMSO)_2]$ [2.3300(9), 2.3343(9), 2.3304(19), and 2.3365(10) Å] with DMSO ligands trans to each other. Replacement of one of the DMSO ligands by an indazole or pyrazole ligand results in a shortening of the other Os−DMSO bond because of a diminished π back-bonding competition between the two trans ligands or decreased σ-directed trans influence of the nitrogen ligand. The S=O bond length of 1.495(2) Å in **2** is equal within 3σ with that of metal-free DMSO [1.492(1) Å], whereas it is 5σ shorter in **3** [1.482(2) Å]. It should, however, be noted that the X-ray diffraction studies for **2** and **3** were performed at different temperatures (Table 1). The crystal structures of **2** and **3** consist of azolium cations and complex anions, which are involved in hydrogen bonding interactions. Two such hydrogen bonds, a weak N3−H···Cl3 [N3−H = 0.88 Å, H···Cl3 = 2.672 Å, N3···Cl3 3.134 Å, ∠N3HCl3 = 113.94°] and a strong N4−H···O1 [N4−H = 0.88 Å, H···O1 = 1.905 Å, N4···O1 = 2.750 Å, ∠N4HO1 = 160.41°] in **2**, are shown in Figure 4, whereas two others, N6−H···O1 [N6−H = 0.86 Å, H···O1 = 1.874 Å, N6···O1 = 2.733 Å, ∠N6HO1 = 176.27°] and a bifurcated hydrogen bond involving N7H as the donor and Cl1 and Cl2 as acceptors [N7−H = 0.86 Å; H···Cl1 = 2.722 Å, N7···Cl1 = 3.378 Å, ∠N7HCl1 = 134.13°; H···Cl4 = 2.876 Å, N7···Cl4 = 3.319 Å, ∠N7HCl4 = 113.88°], in **3** are shown in Figure 5. The results of X-ray diffraction studies of the crystal structures of **5** and **6** are shown in Figures 6 and 7, respectively. Selected bond distances (Å) and bond angles (deg) are quoted in the legends to Figures 6 and 7.

The asymmetric unit of **5** contains an essentially octahedral anion [*trans*-$RuCl_4$(Hbzim)(DMSO)]$^-$ and the $(Ph_3PCH_2Ph)^+$ cation, whereas that of **6** consists of two crystallographically distinct [*trans*-$RuCl_4$(Him)(DMSO)]$^-$ anions, two imidazolium cations, and a disordered ethanol molecule. The osmium(III) atoms in **5** and **6** are bound to four chlorido ligands in the equatorial plane and to DMSO and benzimidazole or imidazole molecules in axial positions. The N2−H group of the benzimidazole ring in **5** appears to form a bifurcated hydrogen bond involving $O1^i$ as well as $Cl4^i$ (N2−H 0.86 Å, H···$O1^i$ = 2.029 Å, N2···$O1^i$ = 2.795 Å, ∠N2HO1^i = 147.81°; N2−H 0.86 Å, H···$Cl4^i$ = 2.827 Å, N2···$Cl4^i$ = 3.412 Å, ∠N2HCl4^i = 126.82°) (Figure 6). Bond lengths and angles in the $(Ph_3PCH_2Ph)^+$ cation are similar to those reported in the literature.[35]

A fragment of the solid-state structure of **7** shown in Figure 8 features an S-bonded DMSO ligand trans to the N-donor atom of Htrz. The Os1−S1 bond distance is 2.2592(8) Å, and the S1−O1 bond length is 1.492(2) Å. The first bond is shorter than Ru1−S1 [2.2730(8) Å] in (Ph_3PCH_2Ph)[*trans*-$RuCl_4$(Htrz)(DMSO)].[16] The latter bond is practically identical to that in free DMSO [1.492(1) Å].[36] The distribution of electron density over the triazole ring indicates a prevailing double bond character of N1−C5 and N2−C3. The analysis of the crystal structure of **7** showed the presence of hydrogen bonding interactions with participation of triazole-

(31) (a) Alessio, E. *Chem. Rev.* **2004**, *104*, 4203−4242.
(32) Chiorescu, I.; Stepanenko, I. N.; Arion, V. B.; Krokhin, A. A.; Scaffidi-Domianello, Y. Y.; Keppler, B. K., manuscript in preparation.
(33) Rudnitskaya, O. V.; Buslaeva, T. M.; Stash, A. I.; Kisin, A. V. *Russ. J. Coord. Chem.* **1995**, *21*, 136−140.
(34) Stepanenko, I. N.; Cebrián-Losantos, B.; Arion, V. B.; Krokhin, A. A.; Nazarov, A. A.; Keppler, B. K. *Eur. J. Inorg. Chem.* **2007**, 400−411.
(35) Cifuentes, M. P.; Waterman, S. M.; Humphrey, M. G.; Heath, G. A.; Skelton, B. W.; White, A. H.; Perera, M. P. S.; Williams, M. L. *J. Organomet. Chem.* **1998**, *565*, 193−200.
(36) Calligaris, M.; Carugo, O. *Coord. Chem. Rev.* **1996**, *153*, 83−154.

Table 2. Cyclic Voltammetric Data for Complexes **2**−**4**, **6** and **7** in Aqueous Phosphate Buffer (pH 7)

complex	$E_{1/2}$ ($Os^{II/III}$)[a], (ΔE_p)[b]	$E_{1/2}$ ($Os^{III/IV}$)[a], (ΔE_p)[b]	ΣE_L/V vs NHE	pK_a(H_2azole$^+$)
2	0.17 (60)	1.41 (70)	-0.23	1.25
3	0.16 (60)	1.40 (70)	-0.29	2.64
4	0.12 (70)	1.27 (60)	-0.39	5.63
6	0.12 (60)	1.33 (80)	-0.37	6.65
7	0.15 (80)	1.35 (70)	-0.31	2.55

[a] Potentials $E_{1/2}$ ($E_{1/2} = (E_{pa} + E_{pc})/2$, where E_{pa} and E_{pc} are the anodic and cathodic peak potential, respectively) are given in V and measured at a scan rate 0.2 V s^{-1} in aqueous phosphate buffer (pH 7) using methyl viologen ($E^{ox}_{1/2} = -0.44$ V vs NHE in water) as internal standard and are quoted relative to NHE. [b] ΔE_p values ($\Delta E_p = E_{pa} - E_{pc}$) are given in mV.

ring nitrogen atoms N2 and N4. The first one acts as an acceptor in the hydrogen bond N8−H···N2 with the following parameters: N8−H = 0.88 Å, H···N2 = 2.089 Å, N8···N2 = 2.811 Å, ∠N8HN2 = 138.71°. The second acts as a donor in the hydrogen bond N4−H···Cl2 ($-x + 1$, $-y$, $-z$) with the following parameters: N4−H = 0.88 Å, H···Cl2 = 2.538 Å, N4···Cl2 = 3.350 Å, ∠N4HCl2 = 153.91°. All of this indicates that, in contrast to [*trans*-$RuCl_4$(Htrz)(DMSO)]$^-$ where 1*H*-1,2,4-triazole is coordinated to ruthenium(III) via N4, the triazole ligand in **7** is stabilized as a 4*H* tautomer. Hence, coordination of triazole via N1 (or N2 in the nomenclature used for 1*H*- or 4*H*-1,2,4-triazole) is proposed. The N2 atom in triazole is less basic than N4,[37] therefore such behavior is rather unexpected. 1,2,4-Triazole behaves as a monodentate ligand coordinating to the first-row or second-row transition metal ion in the majority of cases via N4 ([$Mn^{II}(SO_4)$(Htrz)$(H_2O)_4$],[38] [Cd$(NCS)_2$(Htrz)$_2$],[39] [$FeCl_3$(bpy)(Htrz)],[40] or Zn(II) in human carbonic anhydrase.[41] Only in two cases, namely, (H_2trz)[*cis*-$RuCl_4$(Htrz)$_2$] and (Ph_3PCH_2Ph)[*trans*-$RuCl_4$(Htrz)$_2$], has crystallographic evidence for coordination via N2 been provided.[42]

Electrochemical Behavior in Aqueous Phosphate Buffer at pH 7. The cyclic voltammograms of **2**−**4**, **6**, and **7** in 0.2 M phosphate buffer (pH 7) at a carbon-disk working electrode and at a scan rate of 0.2 V/s display one reversible, single-electron oxidation wave (I^{ox}) assigned to the $Os^{III} \rightarrow Os^{IV}$ process with $E^{ox}_{1/2}$ potential values ranging from 1.27 to 1.41 V and one reversible single-electron reduction wave (I^{red}) attributed to the $Os^{III} \rightarrow Os^{II}$ process with $E^{red}_{1/2}$ potential values ranging from 0.12 to 0.17 V versus NHE (Table 2). The redox potentials of the complexes are in the following rank order: $E_{1/2}$(**2**) > $E_{1/2}$(**3**) > $E_{1/2}$(**7**) > $E_{1/2}$(**6**) ≥ $E_{1/2}$(**4**) (in the case of $Os^{III} \rightarrow Os^{II}$ process $E_{1/2}$(**4**) = $E_{1/2}$(**6**)), which agrees well with the relative electron-donor character of the N-ligands [E_L(Hind) > E_L(Hpz) > E_L(Htrz) > E_L(Him) > E_L(Hbzim)] and their basicity [pK_a(H_2ind$^+$) < pK_a(H_2trz$^+$) < pK_a(H_2pz$^+$) < pK_a(H_2bzim$^+$) < pK_a(H_2im$^+$)][43−46] (Table 2). The reversible responses are characterized by a peak-to-peak separation (ΔE_p) of 60−80 mV and an anodic peak current (i_{pa}) that is almost equal to the cathodic peak current (i_{pc}), as expected for reversible electron-transfer processes. The one-electron nature of electron-transfer processes was verified by comparing the peak-current height (i_p) with that of standard methyl viologen couples under identical experimental conditions.

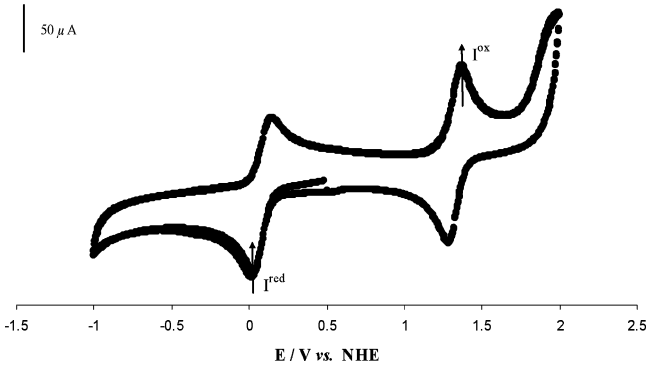

Figure 9. Multiple cyclic voltammogram of 0.5 mM (H_2trz)[*trans*-$OsCl_4$(Htrz)(DMSO)] in aqueous phosphate buffer at pH 7 at a carbon-disk working electrode and at a scan rate of 0.2 V/s, starting with a scan in cathodic direction.

The linear relationships between the redox potentials for the $Os^{III} \rightarrow Os^{II}$ and $Os^{III} \rightarrow Os^{IV}$ processes and $\sum E_L$ (E_L(Cl) = −0.24,[47] E_L(DMSO) = 0.47,[48] E_L(Hind) = 0.26,[16] E_L(Hpz) = 0.20,[48] E_L(Htrz) = 0.18,[48] E_L(Hbzim) = 0.1,[47] E_L(Him) = 0.12[48]), expressed by general Lever's equation[48] (eq 1)

$$E = S_M \sum E_L + I_M \quad (1)$$

and was obtained from the plots in Figures 10 and 11. This expression enabled for the first time the estimate of the S_M and I_M values, which are dependent upon the metal and redox couple, the spin state, and the stereochemistry for the $Os^{II/III}$ (eq 2) and $Os^{III/IV}$ (eq 3) redox couples in aqueous phosphate buffer at pH 7 as follows:

$$E(Os^{II/III}) = 0.35 \sum E_L + 0.26 \quad (2)$$

$$E(Os^{III/IV}) = 0.82 \sum E_L + 1.61 \quad (3)$$

(37) Meot-Ner, M.; Liebman, J. F.; Del Bene, J. E. *J. Org. Chem.* **1986**, *51*, 1105−1110.
(38) Gorter, S.; Engelfriet, D. W. *Acta Crystallogr.* **1981**, *B37*, 1214−1218.
(39) Haasnoot, J. G.; De Keyzer, G. C. M.; Verschoor, G. C. *Acta Crystallogr.* **1983**, *C39*, 1207−1209.
(40) Driessen, W. L.; De Graaff, R. A. G.; Vos, J. G. *Acta Crystallogr.* **1983**, *C39*, 1635−1637.
(41) Mangani, S.; Liljas, A. *J. Mol. Biol.* **1993**, *232*, 9−14.
(42) Arion, V. B.; Reisner, E.; Fremuth, M.; Jakupec, M. A.; Keppler, B. K.; Kukushkin, V. A.; Pombeiro, A. J. L. *Inorg. Chem.* **2003**, *42*, 6024−6031.
(43) Reedijk, J. Heterocyclic Nitrogen-Donor Ligands. In *Comprehensive Coordination Chemistry*; Wilkinson, G., Gillard, R. D., McCleverty, J. A., Eds.; Pergamon Press: Elmsford, NY, 1987; Vol. 2, pp 73−98.
(44) Potts, K. T. *Chem. Rev.* **1961**, *61*, 87−127.
(45) Catalán, J.; Claramunt, R. M.; Elguero, J.; Laynez, J.; Menéndez, M.; Anvia, F.; Quian, J. H.; Taagepera, M.; Taft, R. W. *J. Am. Chem. Soc.* **1988**, *110*, 4105−4111.
(46) Reisner, E.; Arion, V. B.; Eichinger, A.; Kandler, N.; Giester, G.; Pombeiro, A. J. L.; Keppler, B. K. *Inorg. Chem.* **2005**, *44*, 6704−6716.
(47) (a) Lever, A. B. P. *Inorg. Chem.* **1990**, *29*, 1271−1285. (b) Lever, A. B. P.; Dodsworth, E. S. *Inorganic Electronic Structure and Spectroscopy*; Wiley: New York, 1999; pp 227−290.
(48) (a) Bacac, M.; Hotze, A. C. G.; van der Schilden, K.; Haasnoot, J. G.; Pacor, S.; Alessio, E.; Sava, G.; Reedijk, J. *J. Inorg. Biochem.* **2004**, *98*, 402−412. (b) Bouma, M.; Nuijen, B.; Jansen, M. T.; Sava, G.; Flaibani, A.; Bult, A.; Beijnen, J. H. *Int. J. Pharm.* **2002**, *248*, 239−246.

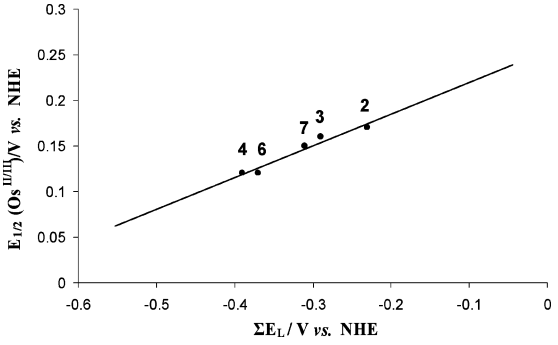

Figure 10. Plot of $E_{1/2}(Os^{II/III})$ for **2**−**4**, **6**, and **7** in aqueous phosphate buffer (pH 7) against $\sum E_L$ (in V vs NHE). $E(Os^{II/III}) = 0.35\sum E_L + 0.26$ ($r = 0.97$) (eq 2). $(H_2ind)[Os^{III}Cl_4(Hind)(DMSO)]$ **2**; $(H_2pz)[Os^{III}Cl_4(Hpz)(DMSO)]$ **3**; $(H_2bzim)[Os^{III}Cl_4(Hbzim)(DMSO)]$ **4**; $(H_2im)[Os^{III}Cl_4(Him)(DMSO)]$ **6**; $(H_2trz)[Os^{III}Cl_4(Htrz)(DMSO)]$ **7**, where $E_L(Hind) = 0.26$; $E_L(Hpz) = 0.20$; $E_L(Hbzim) = 0.10$; $E_L(Him) = 0.12$; $E_L(Htrz) = 0.18$.

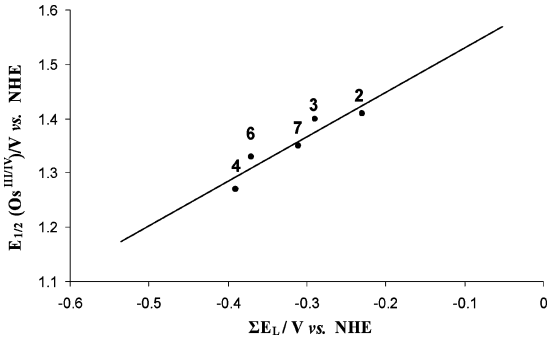

Figure 11. Plot of $E_{1/2}(Os^{III/IV})$ for **2**−**4**, **6**, and **7** in aqueous phosphate buffer (pH 7), against $\sum E_L$ (in V vs NHE). $E(Os^{III/IV}) = 0.82\sum E_L + 1.61$ ($r = 0.93$) (eq 3). $(H_2ind)[Os^{III}Cl_4(Hind)(DMSO)]$ **2**; $(H_2pz)[Os^{III}Cl_4(Hpz)(DMSO)]$ **3**; $(H_2bzim)[Os^{III}Cl_4(Hbzim)(DMSO)]$ **4**; $(H_2im)[Os^{III}Cl_4(Him)(DMSO)]$ **6**; $(H_2trz)[Os^{III}Cl_4(Htrz)(DMSO)]$ **7**, where $E_L(Hind) = 0.26$; $E_L(Hpz) = 0.20$; $E_L(Hbzim) = 0.10$; $E_L(Him) = 0.12$; $E_L(Htrz) = 0.18$.

Resistance to Hydrolysis in Aqueous and Physiological Media. The aqueous solution behavior with respect to hydrolysis of **2**−**4**, **6**, and **7** was studied at 298 K over 48 h by UV−vis spectroscopy and ^{1}H NMR spectroscopy. All of the complexes were quite stable in aqueous solution, as can be seen from their electronic absorption spectra (Figures S2−S6). Immediate hydrolysis can be excluded by comparison of UV−vis spectra of the complexes in methanol and water. In addition, the negative ion ESI mass spectra of complexes **2**−**4**, **6**, and **7** in methanol/water (30/70) showed a similar pattern with three different peaks, which can be attributed to $[Os^{III}Cl_4(L)(DMSO)]^-$, $[Os^{III}Cl_4(DMSO)]^-$, and $[Os^{III}Cl_4]^-$, where L is the respective azole ligand. The presence of the parent peak due to $[Os^{III}Cl_4(azole)(DMSO)]^-$ provides further evidence against immediate hydrolysis of the complexes studied in aqueous solution (Figure S8).

^{1}H NMR experiments in aqueous solution (D_2O, pH ∼5.5, 37 °C) and in physiological medium (phosphate buffer 0.05 M, pH 7.4; NaCl 0.15 M, 37 °C) were carried out with **6** for direct comparison with the earlier reported data for $[Ru^{III}Cl_4(Him)(DMSO)]^-$ (NAMI-A).[48] Because of the paramagnetism of the Os^{III} ion (d^5, low spin), a full identification of the NMR signals was not accomplished. The main peaks observed were assigned taking into account the NMR spectra of NAMI-A[49] and the osmium(II) complexes *trans*,*cis*,*cis*-$OsCl_2(Him)_2(DMSO)_2$ and *cis*,*fac*-$OsCl_2(Him)(DMSO)_3$.[35] ^{1}H NMR spectra of **6** in D_2O (pH ∼5.5, 37 °C) were monitored over 2 days. The spectra obtained immediately after dissolution of **6** and after 2 days were almost identical. A very small signal (<2%) at 2.63 ppm was attributed to free DMSO. Addition of 1 μL of DMSO resulted in an increase of this signal. The integration of the DMSO signal observed for a freshly prepared solution of **6** after 2 days showed an increase of only 3%, indicating that a very small amount of the expected hydrolysis product $[OsCl_4(Him)(H_2O)]^-$ is presumably formed. In contrast, NAMI-A under similar conditions hydrolyzes to a larger extent with formation of the complex $[RuCl_4(Him)(H_2O)]^-$. However, no hydrolysis of Ru−Cl bonds was found. The ^{1}H NMR spectrum of the anion $[OsCl_4(Him)(DMSO)]^-$ showed a broad signal centered at −20 ppm attributed to the protons of S-bonded DMSO (by comparison with the spectrum of **1**), two broad resonances around −17 and −15 ppm (Him, $H_{4,5}$), and a sharper resonance at −5.26 ppm (Him, H_2). Two sharp signals at δ 8.61 and 7.39 ppm (1:2 integration ratio) correspond to H_2 and $H_{4,5}$ of the H_2im^+ counterion, respectively. Other peaks observed in the ^{1}H NMR spectrum of **6** have not been identified (a sharp peak at 7.67 ppm shifted to 7.38 ppm after 2 days, a very broad signal at about 3.38 ppm, a peak at 3.58, and a sharp signal at 2.13 ppm). All of these peaks were of marginal intensity in the spectrum of freshly prepared solutions of **6** and did not change their intensity after 2 days.

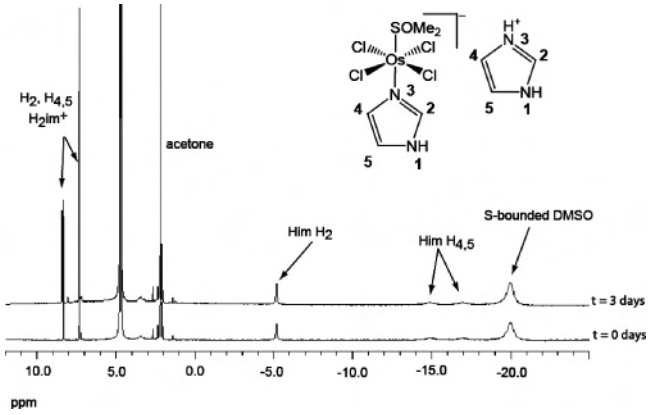

Figure 12. ^{1}H NMR spectra of **6** (5.5 mM) in phosphate buffer (0.05 M phosphate, 0.15 M NaCl), pH 7.4, 37 °C for $t = 0$ and 3 days with chemical formula and atom numbering scheme. For signal integration, acetone (1 μL/mL) was added to the buffer solution as reference (2.16 ppm).

^{1}H NMR spectra of **6** in physiological medium (phosphate buffer 0.05 M, pH 7.4; 0.15M NaCl, 37 °C) were monitored over 3 days. The ^{1}H NMR spectra recorded immediately after dissolution ($t = 0$) and after 3 days were practically identical, as can be seen in Figure 12. Acetone (1 μL/mL) was used as reference, as it gives a sharp signal at 2.16 ppm that does not overlap with the signals of **6**. The integration of the DMSO signal observed (2.66 ppm) for a freshly prepared solution of **6** after 3 days showed an increase of only 5%. The spectrum showed a broad signal centered at −20 ppm for the protons of S-bonded DMSO, two broad bands around −17 and −15 ppm (Him, $H_{4,5}$), and a sharper peak at −5.18 ppm (Him, H_2). The signals of the H_2im^+ counterion seen at 8.33 and 7.30 ppm (1:2 integration ratio) correspond to H_2 and $H_{4,5}$, respectively. Two other minor peaks at 3.42

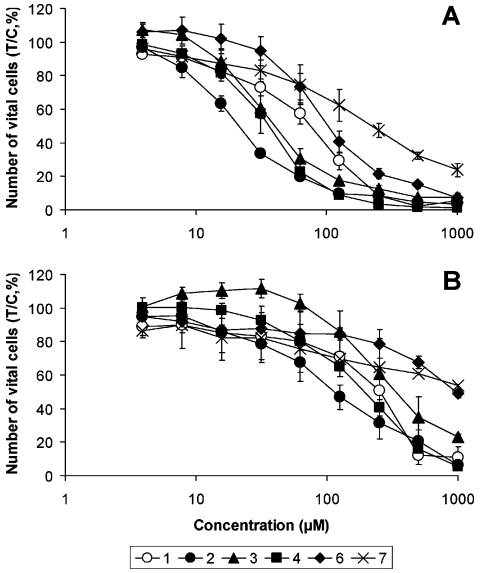

Figure 13. Antiproliferative effects of **1**−**4**, **6**, and **7** in the human cancer cell lines HT-29 (A) and SK-BR-3 (B). Concentration-effect curves were obtained by the MTT assay; values are means ± standard deviations from at least three independent experiments.

and 1.37 ppm have not been identified, but remained unchanged over 3 days. The ^{1}H NMR spectrum of NAMI-A (−15 ppm for S-bonded DMSO, −3.5, −5.6, and −7.8 ppm for coordinated Him, and 8.69 and 7.49 ppm for H_2im^+) showed notably downfield-shifted signals when compared to **6**. Moreover, the ^{1}H NMR spectrum of NAMI-A in physiological medium was time dependent and showed fast replacement of the coordinated chloride and DMSO by water, as evidenced by the appearance of signals at −10 ppm (S-bonded DMSO) and at 0.6 ppm (Him) for *mer*-[$RuCl_3$(Him)-(H_2O)(DMSO)] and free DMSO (2.7 ppm) within a few minutes. NAMI-A underwent chloride and DMSO hydrolysis responsible for the disappearance of NAMI-A after only 15 min.[49a] In contrast, the osmium NAMI-A analogue remained intact after 3 days in physiological medium.

^{1}H NMR spectra of a mixture of **6** and 9-methyladenine (as a DNA model base) in 1:1.5 molar ratio in phosphate buffer (pH 6.0, 37 °C) were measured. The absence of a new set of signals expected for coordinated 9-methyladenine even after 4 days indicated inertness of **6** toward the purine nucleobase under the conditions employed (Figure S7).

Antiproliferative Activity. 1−**4**, **6**, and **7** were tested for their antiproliferative activity in two human cancer cell lines using a colorimetric MTT assay. Concentration-effect curves are depicted in Figure 13, and IC_{50} values are listed in comparison with three ruthenium(III) analogues in Table 3. Structure−activity relationships are similar in both cell lines. In the more sensitive cell line HT-29 (colon carcinoma), antiproliferative activity decreases in the following rank order: **2** > **4** ≈ **3** > **1** ≥ **6** > **7**. In the less sensitive cell line SK-BR-3 (mammary carcinoma), the rank order is as follows: **2** > **4** ≥ **1** ≥ **3** > **6** ≥ **7**. Taking **1** as a reference, replacement of one DMSO ligand by indazole or benzimidazole results in increased antiproliferative activity, whereas replacement by imidazole or triazole weakens it. A comparison with ruthenium analogues (presented in a previous paper)[49] reveals that replacement of ruthenium(III) by osmium(III) increases the activity in HT-29 cells in all three pairs of complexes (L = Hind, Him, or Htrz). Whereas IC_{50} values >100 μM indicate that the potencies of the ruthenium analogues are rather modest, osmium confers a reasonable activity with IC_{50} values mostly in the 10^{-5} M range in these cells. This effect is most pronounced in the case of **2** (L = Hind), which is 10 times more potent than its ruthenium congener. These tendencies are not paralleled by the findings in cell line SK-BR-3, however. But generally, the variation of the azole ligand seems to have greater consequences for biological activity in the osmium series than in the ruthenium series. The observed effects are all the more remarkable because of the inertness of these osmium(III) complexes in general and especially their resistance to hydrolysis (even in chloride-free solution) and lack of reactivity toward 9-methyladenine, which sharply contrasts with the behavior of ruthenium analogues, in particular NAMI-A, under comparable experimental conditions.[49] Whereas the antimetastatic activity of NAMI-A in vivo has been attributed specifically to hydrolyzed species, the lack of cytotoxicity observed with various osmium(II) arene compounds has been attributed to either too slow or too rapid hydrolysis, in the latter case resulting in the predominant formation of stable hydroxo-bridged dimers.[5] Even though the latter compounds differ distinctly from those presented here in terms of oxidation state and ligand sphere, it is quite remarkable that our findings conversely suggest that hydrolysis is not at all an essential prerequisite for antiproliferative activity of this class of osmium complexes. This also contrasts with conclusions drawn from the behavior of rhodium and iridium analogues of NAMI-A, the inactivity of which has been attributed to their inertness to hydrolysis.[9,10]

Table 3. Antiproliferative Effects of **1**−**4**, **6**, and **7** and Three Ruthenium(III) Analogues in Two Human Cancer Cell Lines

compound	L	IC_{50} (μM)[a]	
		HT-29	SK−BR-3
1	DMSO	75 ± 11	241 ± 57
2	Hind	21 ± 1	119 ± 41
3	Hpz	39 ± 10	325 ± 141
4	Hbzim	36 ± 2	194 ± 19
6	Him	103 ± 15	930 ± 46
7	Htrz	214 ± 61	>1000
Ru analogues[b]	Hind	212 ± 22	169 ± 10
	Him	339 ± 68	472 ± 25
	Htrz	322 ± 32	415 ± 48

[a] Fifty percent inhibitory concentrations after exposure for 96 h in the MTT assay. Values are means ± standard deviations from at least three independent experiments. [b] Data taken from the previous publication.[49]

NAMI-A reduces the formation and growth of metastases in experimental tumor models but has little impact on the growth of primary tumors.[50] This behavior is in line with a modest cytotoxicity but a pronounced and rapid impact on

(49) Groessl, M.; Reisner, E.; Hartinger, C. G.; Eichinger, R.; Semenova, O.; Timerbaev, A. R.; Jakupec, M. A.; Arion, V. B.; Keppler, B. K. *J. Med. Chem.* **2007**, *50*, 2185−2193.

(50) Sava, G.; Zorzet, S.; Turrin, C.; Vita, F.; Soranzo, M. R.; Zabucchi, G.; Cocchietto, M.; Bergamo, A.; DiGiovone, S.; Pezzoni, G.; Sartor, L.; Garbisa, S. *Clin. Cancer Res.* **2003**, *9*, 1898−1905.

the interactions of tumor cells with the extracellular matrix, suggesting a target located in the cell membrane. In particular, NAMI-A increases actin-dependent cell adhesion by a mechanism probably involving integrin activation,[51,52] it inhibits matrix degradation by reducing the release of matrix metalloproteinases rather than by its direct inhibitory effect on these enzymes,[53] and it reduces cell invasiveness and migration,[50,53,54] altogether manifesting in a less malignant cell phenotype. In endothelial cells, inhibition of proliferation, chemotactic behavior, and matrix metalloproteinase secretion have been observed, suggesting a contribution of antiangiogenic effects to the antimetastatic properties.[55] Furthermore, NAMI-A is capable of inducing a transient cell cycle arrest[55] and binding to DNA to a certain degree,[56] but neither of these effects is likely to account for the antimetastatic activity.

NAMI-A is transformed under physiological conditions into several different ruthenium species, but their individual contributions to the pharmacological effects remain elusive.[48a,57] Rapid hydrolysis to polyoxo species in physiological buffer, their higher cellular uptake, and their unaltered effects on the cell cycle of metastatic cells have prompted investigators to attribute the activity of NAMI-A to hydrolysis products.[48a] Furthermore, reduction to ruthenium(II) species does not alter the effects on cell cycle distribution and metastasis growth to a meaningful extent.[57] Because it remains unclear which molecular effects account for the antimetastatic activity and whether they depend on hydrolysis and/or reduction, it is impossible to predict whether this activity is preserved in the osmium analogues. Experiments in suitable rodent tumor models with reliable metastasizing propensity are planned in order to examine these compounds for their antimetastatic capacity, along with their impact on primary tumors in vivo. From a therapeutical point of view, a compound endowed with a dual mechanism combining inhibitory effects on the processes of tumor cell invasion and migration with a cytotoxic component in primary as well as secondary sites of malignant tumors would be particularly attractive for further development. In any case, the suggestion of Messori et al. to use analogues not amenable to hydrolysis as model compounds for studying the biodistribution profile of unhydrolysed NAMI-A[10] is applicable also to the osmium complexes presented here.

Final Remarks. Investigation of stepwise reduction of OsO_4 with $N_2H_4 \cdot 2HCl$ and $SnCl_2 \cdot 2H_2O$/DMSO enabled the preparation and characterization of $[(DMSO)_2H][trans\text{-}Os^{III}Cl_4(DMSO)_2]$, the compound which remained elusive (at least in terms of solid-state isolation) for quite a long time. The latter proved to be a suitable precursor for the synthesis of osmium NAMI-A analogues, which showed reasonable antiproliferative activity in vitro. The full characterization of prepared compounds, both in the solid state and in solution, permitted the elucidation of essential differences between related osmium and ruthenium complexes. In particular, we found that osmium complexes, which are markedly more inert than related ruthenium compounds toward substitution reactions (hydrolysis, interaction with DNA bases), in accord with their position in the periodic table, partially show a higher antiproliferative activity than the related ruthenium compounds. This is even more intriguing, if we take into account that other related compounds based on iridium and rhodium do not exhibit any antiproliferative activity.

The slope, S_M, and intercept, I_M, of Lever's equation were determined for the Os^{II}/Os^{III} and Os^{III}/Os^{IV} couples in aqueous medium, which will allow the prediction of the redox potential of other osmium complexes with the same redox couples.

The work also made a notable crystallographic contribution. **2**, **3**, and **5**−**7** expand the relatively small class of Os^{III}−DMSO-azole complexes characterized by X-ray diffraction. The binding mode of triazole (monofunctional via N2) and the tautomer stabilized (4*H*) are distinct from those found in related ruthenium compounds (coordination via N4 and 1*H* tautomer).

Acknowledgment. We thank A. Roller for collection of X-ray data and Dr. S. Shova for discussion of the crystallographic part of the work.

Supporting Information Available: UV−vis spectra of complexes $[H_2L][MCl_4(HL)(DMSO)]$, where M = Os, Ru, UV−vis spectrum of **1** in water, UV−vis spectra of **2**−**4**, **6**, and **7** in water monitored over 48 h, ^{1}H NMR spectrum of **6** with 9-MeAde, ESI mass spectrum of **6** in methanol/water (30/70), X-ray crystallographic files in CIF format for **1**−**3**, **5**, **6**, and **7**. This material is available free of charge via the Internet at http://pubs.acs.org.

IC700405Y

(51) Sava, G.; Frausin, F.; Cocchietto, M.; Vita, F.; Podda, E.; Spessotto, P.; Furlani, A.; Scarcia, V.; Zabucchi, G. *Eur. J. Cancer* **2004**, *40*, 1383−1396.
(52) Frausin, F.; Scarcia, V.; Cocchietto, M.; Furlani, A.; Serli, B.; Alessio, E.; Sava, G. *J. Pharmacol. Exp. Ther.* **2005**, *313*, 227−233.
(53) Pacor, S.; Zorzet, S.; Cocchietto, M.; Bacac, M.; Vadori, M.; Turrin, C.; Gava, B.; Castellarin, A.; Sava, G. *J. Pharmacol. Exp. Ther.* **2004**, *310*, 737−744.
(54) Zorzet, S.; Bergamo, A.; Cocchietto, M.; Sorc, A.; Gava, B.; Alessio, E.; Iengo, E.; Sava, G. *J. Pharmacol. Exp. Ther.* **2000**, *295*, 927−933.
(55) Vacca, A.; Bruno, M.; Boccarelli, A.; Coluccia, M.; Ribatti, D.; Bergamo, A.; Garbisa, S.; Sartor, L.; Sava, G. *Br. J. Cancer* **2002**, *86*, 993−998.
(56) Pluim, D.; van Waardenburg, R. C. A. M.; Beijnen, J. H.; Schellens, J. H. M. *Cancer Chemother. Pharmacol.* **2004**, *54*, 71−78.
(57) Sava, G.; Bergamo, A.; Zorzet, S.; Gava, B.; Casarsa, C.; Cocchietto, M.; Furlani, A.; Scarcia, V.; Serli, B.; Iengo, E.; Alessio, E.; Mestroni, G. *Eur. J. Cancer* **2002**, *38*, 427−435.